Influence of landscape configuration on the sediment retention of Mt. Makiling Forest Reserve, Philippines: An analysis of model-generated land cover

Nico R. Almarines^{1*}, Nathaniel C. Bantayan¹, Canesio D. Predo¹, Pastor L. Malabrigo Jr.²

¹Institute of Renewable Natural Resources, University of the Philippines Los Baños, College, Laguna, Philippines; *Email: nralmarines@up.edu.ph ²Department of Forest Biological Sciences, University of the Philippines Los Baños, College, Laguna, Philippines

ABSTRACT. Sediment retention is among the most important ecosystem services impacted by anthropogenic drivers of land cover change. However, there have been few efforts to gauge the impacts of land cover configuration on the total ecosystem sediment retention in a landscape. The study aims to do so by computing changes in landscape pattern metrics of catchments draining from the Mt. Makiling Forest Reserve (MMFR) using FRAGSTATS. Then, changes in sediment retention index (SRI) were modeled with the InVEST sediment delivery ratio (SDR) model. Statistical analysis of 64 landscape pattern metrics vis-à-vis SRI using a spatial error model showed eight class-level metrics statistically significant at $\alpha = 0.05$. These were the edge density (ED) of built-up areas ($\beta = -0.0039$), perennial crops ($\beta = 0.0025$), and grasslands ($\beta = 0.0102$); the disjunct core area density (DCAD) annual crops ($\beta = 0.0243$), grasslands ($\beta = -0.0064$), perennial crops ($\beta = -0.0068$); and the mean radius of gyration (GYRATE) of perennial crops ($\beta = 0.0002$) and annual crops ($\beta = 0.0003$). However, despite this statistical significance, less than 5% of changes in SRI can be attributed to landscape configuration. This indicates that while landscape configuration influences sediment retention, landscape composition or land cover area remains an important predictor of sediment retention.

Keywords: landscape metrics, landscape pattern, sediment retention, spatial error model

INTRODUCTION

Human-induced land use and land cover dynamics often result in considerable risks to ecology and human well-being (Adepoju *et al.*, 2019; Moanga, 2020). Such changes could disrupt landscape patterns, interfere with ecological processes, compromise the landscape's functional integrity, and decrease ecosystem services (Hasan *et al.*, 2020; Martello *et al.*, 2023). Thus, effective landscape management is contingent on understanding the linkages between landscape patterns and ecosystem services (Duarte *et al.*, 2018; Qiu *et al.*, 2018; Saidi & Spray, 2018; Loc *et al.*, 2020; Dong *et al.*, 2022).

Landscape patterns depict the various aspects of spatiotemporal heterogeneity of an inherently complex landscape and are usually quantified using algorithms called landscape pattern metrics (McGarigal, 2012; Remmel & Mitchell, 2021). These metrics comprise composition and configuration (Abdolalizadeh *et al.*, 2019; Yohannes *et al.*, 2020). Landscape composition is non-spatial and pertains to the number and proportion of land cover classes, while landscape configuration describes the spatial arrangement, position, and orientation of land cover, including the shape and size of patches (Hou & Estoque, 2020; Liu *et al.*, 2020;

Redhead *et al.*, 2020; Fu *et al.*, 2021). These metrics may also be classified according to their use case. Structural metrics, for example, quantify the physical landscape structure without reference to a specific ecological process of species, while functional metrics do so in a particular context and thus, need additional parametrization (McGarigal, 2012; Gustafson, 2019;).

It is well-established that landscape patterns influence ecosystem services, with fragmentation being the most researched factor and known to cause adverse impacts on the supply of ecosystem services (Fu et al., 2013; Mitchell et al., 2015; Hasan et al., 2020). A metaanalysis of 121 journal articles showed that different aspects of landscape patterns influence water quality, disease control, pest control, pollination, and aesthetic ecosystem services (Duarte et al., 2018). Similarly, the structure of urban green spaces seems to affect urban microclimate and promises to improve the mitigation of urban heat islands (Du et al., 2019; Hou & Estoque, 2020; Li et al., 2021; Gao et al., 2022). Biodiversity and habitat quality are also affected by landscape patterns (Zhang et al., 2022). Interestingly, some studies also aim to relate landscape patterns as crop and ecological resilience indicators to climate change (Cushman & McGarigal, 2019; Honkaniemi et al., 2020; Redhead et al., 2020).

While there are numerous studies on the influence of landscape patterns on soil erosion and sediment export, most of these tend to focus on landscape composition (Srichaichana et al., 2019; Bouguerra et al., 2020; Hasan et al., 2020; Negese, 2021; Li et al., 2022a; Li et al., 2022b). Comparatively, the impact of landscape configuration on the sediment retention services of ecosystems has been less extensively examined-especially in the Philippine context (Duarte et al., 2018). Research studies of this nature, however, do not always measure the linkages between landscape configuration and sediment retention, but those that do, demonstrate the need to quantify such interactions (Ahmadi et al., 2018; Yohannes et al., 2020; Xia et al., 2021; Martello et al., 2023). Particularly, it is important to identify what variables or landscape pattern metrics would significantly influence the magnitude of changes in sediment retention. Hence, the study aimed to assess how changes in landscape configuration affect the degree of ecosystem sediment retention at a catchment level through the quantification and statistical analysis of landscape-level and class-level landscape pattern metrics and the sediment retention index.

METHODOLOGY

Study area

The study was modeled in the watersheds along the southern portion of Laguna de Bay which intersects with the MMFR or the Mt. Makiling Forest Reserve. MMFR is a protected area along the southwestern part of the Island of Luzon, about 60 km southeast of Metro Manila, and was designated as an ASEAN Heritage Park in 2013 (Castillo et al., 2021). The watersheds it intersects play a significant role with local communities and ecosystems within its catchments through the provisioning of ecosystem services (Paelmo et al., 2015; Clanor et al., 2016; Spiegelberg et al., 2017). It is also an important reservoir of biological resources, covering a variety of ecosystems, including lowland evergreen rainforests and lower montane forests which have yielded high floristic, faunal, fungal, and microbial diversity (Nacua et al., 2018; Arguelles, 2019; Gonzalez et al., 2020; Magcale-Macandog et al., 2022).

The study looked at 15 watersheds intersecting with the MMFR ranging from 88 ha to almost 20,000 ha draining into the Laguna de Bay (**Figure 1**). These were delineated from an Interferometric Synthetic Aperture Radar (IfSAR) derived 5 m Digital Terrain Model (DTM) provided by the National Mapping and Resource Information Authority (NAMRIA) in 2016. ArcHydro was used in delineating and subdividing the watersheds into 207 individual catchments. This used an eight-direction flow model (D8) and a 40,000-pixel threshold value equivalent to 100 ha or 1 km2. Most of these catchments (60%) are at most 2 km², and 37% are less than 1 km². The average catchment perimeter is 10.11 km, with an average basin length of 3.42 km.

Landscape pattern metrics

The program FRAGSTATS was used to assess and quantify landscape pattern metrics. It provides detailed statistical information on various landscape metrics at different scale levels. However, for this study, 14 landscape pattern metrics were used for landscape pattern analysis of each catchment in the study area (Table 1). All 14 metrics are structural metrics that measure landscape configuration. The details of each landscape pattern metric used in the study are described in **Annex 1**. These can be grouped according to their utility, as many tend to measure similar attributes of landscape patterns. As the name suggests, area-edge metrics describe the size and density of patches and the extent of their edge in the landscape; they are among the most fundamental metrics in landscape ecology (McGarigal, 2015). Core area metrics are similar to area-edge metrics but also account for edge effects;

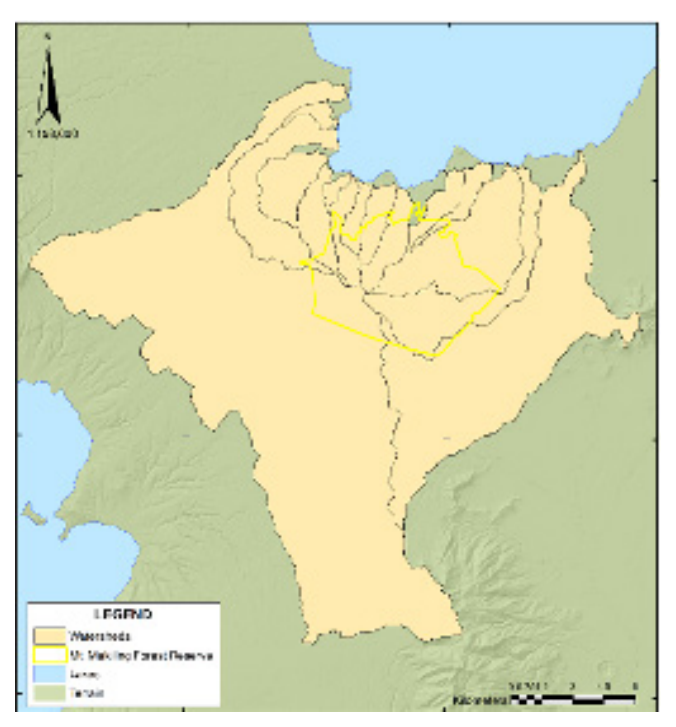


Figure 1. Location map of the study area.

contagion-interspersion metrics describe the level of land cover fragmentation and aggregation (McGarigal, 2012). Lastly, connectivity metrics look at how well-linked and enmeshed each patch type of the landscape mosaic is, while diversity metrics describe the degree of heterogeneity in the landscape (Duarte *et al.*, 2018).

Table 1. List of landscape fragmentation metrics used in the study.

Type of metric	Landscape metric	Abbreviation
Area-edge metrics	Patch density	PD
	Edge density	ED
	Mean radius of gyration	GYRATE
	Largest patch index	LPI
Core area metrics	Disjunct core area density	DCAD
Contagion-	Contagion index	CONTAG
Interspersion metrics	Aggregation index	Al
metrico	Landscape division index	DIV
	Splitting index	SPLIT
Connectivity metrics	Patch cohesion index	COHES
Diversity metrics	Patch richness	PR
	Patch richness density	PRD
	Shannon's diversity index	SHDI
	Simpson's diversity index	SDI

Aside from the landscape-level metrics, class-level metrics were also computed. These are like landscape-level metrics but disaggregated by land cover types. Nine landscape pattern metrics were computed for each of the six land cover classes, adding to 45 class-level metrics (**Table 2**).

Sediment retention modeling

The SDR Model of the InVEST software version 3.3.3. was used to quantify and spatially visualize sediment retention under the various land cover configurations. InVEST is a geospatial modeling platform that is one of the most widely used for modeling ecosystem services in historical and future contexts (Agudelo *et al.*, 2020; Gomes *et al.*, 2021; Meraj *et al.*, 2022; Nedkov *et al.*, 2022).

The SDR model estimates the sediment retention service of an ecosystem by comparing the avoided soil loss of a land cover type to bare soil (Hamel *et al.*, 2015; Sharp *et al.*, 2018). This is operationalized in the model through the SRI (Equation 1), which looks at the soil loss of a pixel given a particular rainfall erosivity, soil erodibility, and slope length, and gauges the effect of the vegetative cover and conservation practices by weighing it against its respective sediment delivery ratio (Borselli *et al.*, 2008; Hamel *et al.*, 2017; Sharp *et al.*, 2018). This model is particularly practical since it

Metric		Class-level fragmentation metric code					
Wetric	Annual crop	Built-up	Forest	Grassland	Perennial crop		
PD	PD_AC	PD_BU	PD_F	PD_GL	PD_PC		
LPI	LPI_AC	LPI_BU	LPI_F	LPI_GL	LPI_PC		
ED	ED_AC	ED_BU	ED_F	ED_GL	ED_PC		
GYRATE	GYRATE_AC	GYRATE_BU	GYRATE_F	GYRATE_GL	GYRATE_PC		
DCAD	DCAD_AC	DCAD_BU	DCAD_F	DCAD_GL	DCAD_PC		
COHES	COHES_AC	COHES_BU	COHES_F	COHES_GL	COHES_PC		
DIV	DIV_AC	DIV_BU	DIV_F	DIV_GL	DIV_PC		
SPLIT	SPLIT_AC	SPLIT_BU	SPLIT_F	SPLIT_GL	SPLIT_PC		
Al	AI_AC	AI_BU	AI_F	Al_GL	AI_PC		

Table 2. Class-level fragmentation metric codes for each land cover type.

(Equation 1)

$$I_{sr} = R_i K_i \left(S_i \frac{(A_{i-in} + D^2)^{m+1} - A_{i-in}^{m+1}}{D^{m+2} \cdot x_i^m \cdot (22.13)^m} \right) (1 - C_i P_i) SDR_i$$

Where:

 R_i = rainfall erosivity (MJ·mm(ha·hr)⁻¹)

 $K = \text{soil erodibility (ton-ha-hr(MJ-ha-mm)}^{-1})$

 S_i = slope factor computed as $10.8 \cdot \sin(\theta) + 0.03$ where $\theta < 9\%$ or $16.8 \cdot \sin(\theta) - 0.50$, where $\theta \ge 9\%$

 $A_{(i-in)}$ = contributing area (m²) at the inlet of a grid cell

D = grid cell linear dimension (m)

 $x_i = |\sin \alpha_i| + |\cos \alpha_i|$ where α_i is the aspect direction for grid cell i

m = RUSLE length exponent factor

 C_i = crop-management factor

 P_{i} = support practice factor

SDR = sediment delivery ratio

The rainfall erosivity factor (R) was computed using an equation developed by Lee and Lin (2015) which relates annual rainfall erosivity in MJ·mm(ha·hr)⁻¹ to annual average precipitation (Equation 2). This was selected since it was tested to have good agreement with observation data from 10-year rainfall data in 55 stations across Taiwan with over 16,000 recorded storm events and annual precipitations ranging from 1,300 mm to 4,000 mm. To ensure sufficient coverage of the study area for interpolation, Philippine Atmospheric Geophysical and Astronomical Services Administration (PAGASA) climate stations within a 50-km buffer from the centroid of the study area were

identified, and climatic data for each weather station were collected from 1980 to 2010 to compute for the climatological normals of each station and obtain the average annual precipitation data needed to compute for rainfall erosivity. Annual precipitation of nearby stations was well within the range of values from which Equation 2 was developed and tested. An R factor raster was generated by interpolating rainfall erosivity values from the PAGASA climate stations using empirical Bayesian kriging with a thin plate spline semivariogram (Gupta *et al.*, 2017; Javari, 2017; Yang & Xing, 2021).

(Equation 2)
$$R = 2.74P^{1.2}$$

Where: $P = average annual precipitation (mm ha^{-1} yr^{-1})$

Soil erodibility (K) (**Table 3**) was computed for each pixel by utilizing a digital soil map from the Bureau of Soil and Water Management and assigning soil erodibility values of each soil type based on its textural class, and organic matter content (OMC) converted to SI metric units or t-ha-hr (ha-MJ-mm)⁻¹ (Foster *et al.*, 1981; Schwab *et al.*, 1981; Parveen & Kumar, 2012). This was used since the values were empirically calculated based on the soil erodibility nomograph (Wischmeier *et al.*, 1971) and equation (Wischmeier & Meyer, 1973) which is the most widely used method to estimate K-factor and had also been adapted for RUSLE2 (Dabney *et al.*, 2012; Auerswald *et al.*, 2014; Corral-Pazos-de-Provens *et al.*, 2022).

Table 3. K-factor values converted to $t \cdot ha \cdot hr$ $(ha \cdot MJ \cdot mm)^{-1}$ based on soil textural class and OMC.

Soil texture	Average OMC	OMC < 2%	OMC > 2%
Clay	0.02897	0.03161	0.02766
Clay loam	0.03951	0.04346	0.03688
Coarse sandy loam	0.00922	0.00922	0.00922
Fine sand	0.01054	0.01185	0.00790
Fine sandy loam	0.02371	0.02897	0.02239
Heavy clay	0.02239	0.02502	0.01976
Loam	0.03951	0.04478	0.03424
Loamy fine sand	0.01449	0.01976	0.01185
Loamy sand	0.00527	0.00659	0.00527
Loamy, very fine sand	0.05136	0.05795	0.03293
Sand	0.00263	0.00395	0.00132
Sandy clay loam	0.02634	0.02634	0.02634
Sandy loam	0.01712	0.01844	0.01580
Silt loam	0.05005	0.05400	0.04873
Silty clay	0.03424	0.03556	0.03424
Silty clay loam	0.04214	0.04610	0.03951
Very fine sand	0.05663	0.06058	0.04873
Very fine sandy loam	0.04610	0.05400	0.04346

Sources: (Foster et al., 1981; Schwab et al., 1981; Parveen & Kumar, 2012)

Lastly, C factor values were based on two sources, David (1988) and Benavidez et al. (2018). The study uses a land cover dataset which includes a combination of existing and modeled land cover maps from Almarines (2019). Maps for 2010 and 2015 were sourced from NAMRIA. Conversely, the land cover maps for 2020, 2025, 2030, and 2035 were modeled using a hybrid Markov chain-multilayer perceptron neural network (MC-MPNN) model with an accuracy rate of 77.6%. Since the model accuracy is on the lower end of acceptability, the study uses the land cover dataset to determine general trends of land cover patterns in the landscape for SRI computation and statistical analysis. Hence, it also avoids using the dataset to specify likely areas of projected land conversion and inferring the potential impacts of these projected changes because this would require a comprehensive breakdown of the prerequisite stages of land cover projection. These stages include filtering and grouping of historical land cover processes, generation of transition probability matrix, identification of type and influence of driver variables used in each transition submodel, and

generation of transition probability maps; all of which are not within the scope of the study.

All the spatial inputs for the SDR model were converted to 5-m resolution raster grids. Hence, the resulting model outputs also have a 5-m resolution. The summary of all the input data used for SDR modeling is shown in **Table 4**.

Table 4. Data requirements and data sources utilized for the SDR model.

Input data	Source
Digital terrain model	IfSAR-derived DTM from NAMRIA (2016)
Rainfall erosivity	Climatological data from PAGASA climate stations (1980–2010)
	R values computed using Equation 1 (Lee & Lin, 2015)
Soil erodibility	Soil maps from BSWM
	Soil erodibility values from Schwab <i>et al.</i> (1981)
Land cover	2010 and 2015 land cover maps from NAMRIA
	Projected land cover maps were from an MC-MPNN (Almarines, 2019)
Watershed boundary	Delineated from DTM using ArcHydro
C and P factors	Benavidez <i>et al.</i> , 2018; David, 1988

Statistical analysis

Multiple regression was used to assess the relationship between SRI and landscape pattern metrics—landscapelevel and class-level fragmentation metrics. Multiple regression typically follows the formula:

(Equation 3)

$$Y = \beta_0 + \beta_1 X_1 + \beta_2 X_2 + \beta_3 X_3 + \dots + \beta_n X_n$$

Where:

Y = predicted value of the dependent variable

X = predictor or independent variables

 $\beta\Box$ = beta coefficients

Once a regression model was developed, each independent variable's variance inflation factor (VIF) was computed (Equation 4). This allows the detection

of multicollinearity in the regression model, which indicates a correlation between independent variables in the model and, thus, could negatively impact the regression outputs (Miles, 2014). Independent variables with high multicollinearity were removed from the revised regression model (Craney & Surles, 2002).

(Equation 4)

$$VIF_i = \frac{1}{1 - R_i^2}$$

Where:

 VIF_i = variance inflation factor for independent variable i

 R_i^2 = computed R^2 for independent variable i

Spatial autocorrelation was also measured for both the dataset and the revised regression model. The spatial correlation of a variable with itself through space measures how distance influences the variable; this quantifies the presence of systematic spatial variation through similarity and clustering of nearby objects (Dubin, 2003). This is important since spatial patterns may provide insights into underlying factors affecting ecological processes (Lichstein et al., 2002). In addition, a review of a decade of research shows that ecological regression models which do not incorporate spatial autocorrelation tend to misestimate coefficients by 25% (Dormann, 2007). To assess spatial autocorrelation, Moran's I test for global spatial autocorrelation was used (Equation 5). It is based on cross-products of the deviations from the mean and is calculated for observations on a variable at two locations across links (Getis, 2010).

(Equation 5)

$$I = \frac{n}{S_0} \frac{\sum_i \sum_j w_{ij} (x_i - \bar{x}) (x_j - \bar{x})}{\sum_i (x_i - \bar{x})^2}$$

Where:

I = Moran's I

 x_i = predictor or independent variables

 \dot{w}_{ij} = elements of the weight matrix at locations i and i

 S_0 = s the sum of the weight matrix elements equal to $\sum_i \sum_i w_{ii}$

Furthermore, Geary's C statistic (Equation 6) was computed to measure the heteroskedasticity of the model residuals based on the deviations in responses

of each observation with one another (Geary, 1954). Its value is expected to be 1 without autocorrelation regardless of the specified weight matrix (Gunaratna *et al.*, 2013).

(Equation 6)

$$C = \frac{n-1}{2S_0} \frac{\sum_i \sum_j w_{ij} (x_i - x_j)^2}{\sum_i (x_i - \bar{x})^2}$$

Where:

C = Geary's C statistic

 x_i = predictor or independent variables

 w_{ij} = elements of the weight matrix at locations i and j

 S_0 = s the sum of the elements of the weight matrix equal to $\sum_i \sum_i w_{ij}$

If spatial autocorrelation is significant, a spatial regression model will be used. In this case, the spatial error model was used to analyze spatial autocorrelation in the model residuals. It incorporates spatial effects through error terms in the model (Equation 7).

(Equation 7)

$$v = x\beta + (\lambda W\varepsilon + \xi)$$

Where:

y = predicted value of the dependent variable

x = predictor or independent variables

 β = beta coefficient

 λ = spatial error coefficient

 ξ = vector of uncorrelated error terms

 $W\varepsilon$ = vector of error terms, spatially weighted using the weights matrix (W)

RESULTS AND DISCUSSION

Changes in sediment retention

The changes in land cover in the landscape led to changes in the sediment retention index of the catchments in the study area. The InVEST SDR model was used to estimate the SRI of the catchments and simulated the degree of spatial variation in SRI given the land cover for 2010, 2015, 2020, 2025, 2030, and 2035. The univariate statistics (*e.g.*, mean, median, standard deviation, sample variance, kurtosis, skewness, range) of the catchment-level sediment retention index are listed in **Table 5**.

Table 5. Univariate statistics of the modeled catchment sediment retention index

Statistic	Sediment retention index					
Statistic	2010	2015	2020	2025	2030	2035
Mean	0.9914	0.9487	0.9541	0.9516	0.9486	0.9468
Median	0.5439	0.4390	0.4315	0.4298	0.4299	0.4298
Standard deviation	1.2057	1.1716	1.1800	1.1777	1.1723	1.1701
Sample variance	1.4537	1.3726	1.3924	1.3869	1.3743	1.3691
Kurtosis	3.9071	4.4478	4.4907	4.5435	4.6032	4.6177
Skewness	1.8181	1.9040	1.9177	1.9241	1.9238	1.9246
Range	7.0746	7.0819	7.0901	7.0939	7.1273	7.1250

The temporal changes in univariate statistics indicate that the SRI in the landscape decreased from 2010 to 2035. Both the mean and median values showed a decreasing trend. In 2010, the mean SRI of the catchments was 0.99 and had a median value of 0.54; by 2035, this changed to 0.94 and 0.43, respectively. This decreasing trend is evident for all the transition periods except for 2015–2020, where the mean SRI had increased. Moreover, the highly positive skewed SRI data have a growing trend in skewness. This suggests that more catchments have shifted to lower SRI classes. Likewise, kurtosis follows a similar course – becoming increasingly leptokurtic. Thus, it implies that the combined weight of the tails in the SRI dataset (i.e., lower SRI values) has increased relative to the rest of the SRI distribution. Catchment-level net change analysis of the dataset presents a comparable assessment of the temporal shifts in SRI. The frequency distribution of the percent change in SRI of each catchment for all

transition periods is summarized in **Figure 2**. The 2015-2020 period had the greatest net increases in SRI, with 58% of catchments gaining SRI. This period was the only time when more catchments had a net gain in SRI compared to the aggregate number of catchments with either no change or a net loss. The rest of the transition periods are characterized by a predominant net loss in SRI. The highest number of net losses was observed in the 2025-2030 period; 68% of the catchments had a net decrease in SRI. This was followed by the 2020-2025 and 2030-2035 transition periods, with a net decrease of 66% and 65% of catchments, respectively.

The spatial distribution of net changes in SRI was also visually evaluated since maps of absolute SRI values did not show any clear trend in SRI (Figure 3). The maps of net SRI changes suggest a certain degree of spatial clumping of catchments with increases in SRI and with SRI decline. Hence, this may indicate spatial autocorrelation, which needs to be tested in the statistical analysis.

General trends in landscape composition

While landscape composition is not a part of the analysis, it is still important to look at its general trends to understand the general changes in the landscape since this affects sediment retention. While initially, the landscape was more than 30% annual crops in 2012 and 30% perennial crops in 2015, the projected maps showed trends in land cover change which would make built-up areas the more expansive land cover type by 2035 – covering 37% of the area (**Figure 4**). Built-up areas expanded by 4,261 ha, a 35% increase. This increase is fueled by the conversion of both annual crops and perennial crops into built-up. Annual crops decreased their overall coverage to 16%, a net decrease of 70%

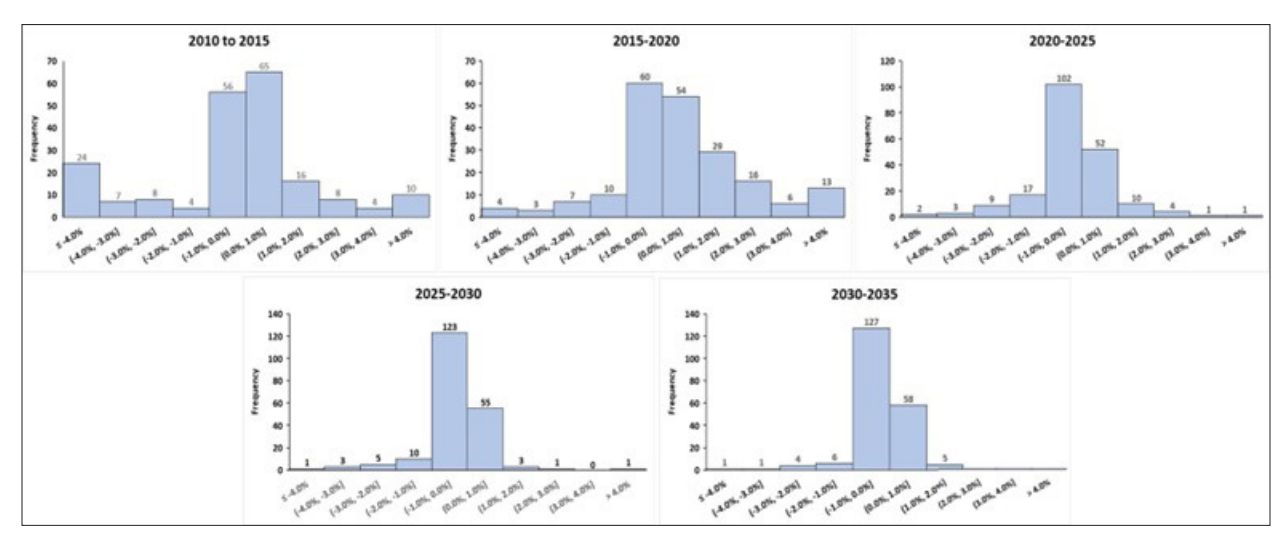


Figure 2. Summary of changes in SRI in the five transition periods.

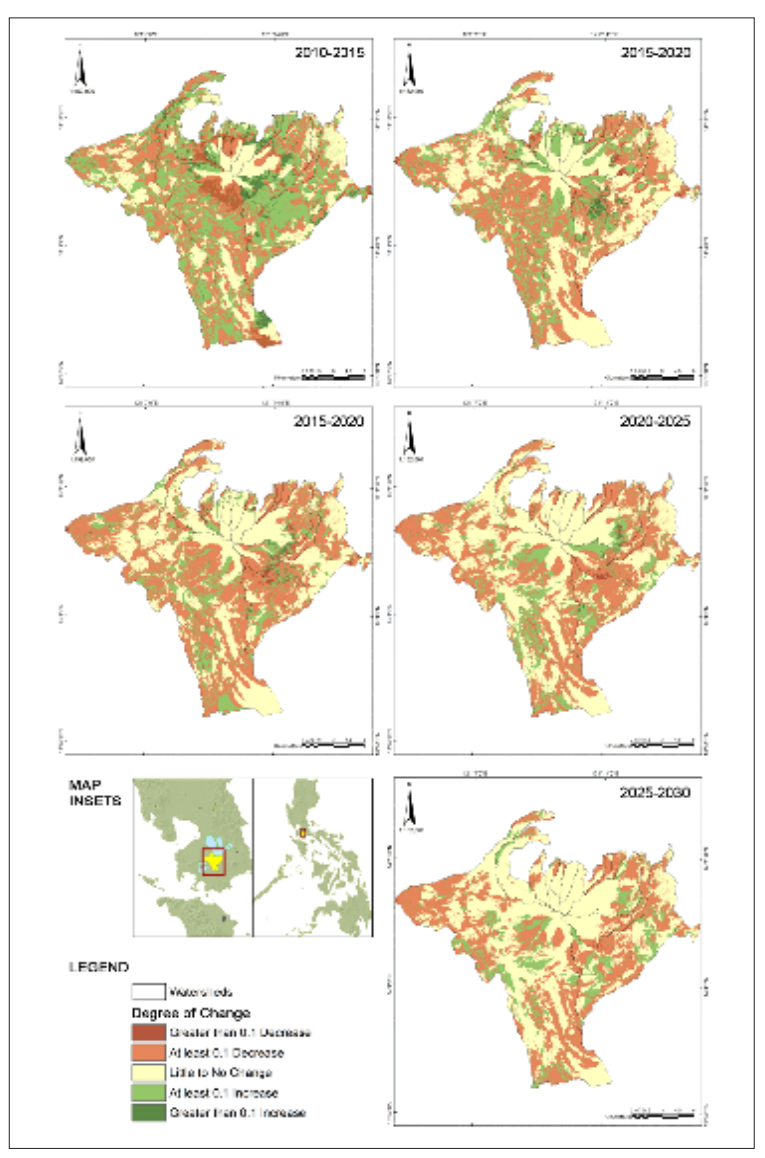


Figure 3. Spatial changes in SRI from 2010 to 2035.

or around 4,126 ha. Furthermore, the two-percentage point net contraction of perennial crops constitutes a 6% decrease in its total area. The areas of inland water and forest cover persisted through the prediction years since they were not included in the model (Almarines, 2019). Finally, the area of grasslands increased to 9% of the landscape and showed an 18% net gain of 619 ha. All these trends show that vegetation decreased in the modeled land cover maps and is likely the cause of the decrease in SRI.

Changes in landscape configuration

The mean and median values of both Patch Density (PD) and Edge Density (ED) increased during the period (**Figure 5**). PD had a net increase of 257% in mean values and a net gain of 325% in median values

from 2010 to 2030, with the highest values computed for 2025. Similarly, ED has a 169% and 195% net gain in mean and median values, respectively, from 2010 to 2030. The trends in PD and ED indicate that the land cover pattern had been increasingly fragmented through time, with patches becoming more prevalent in the study area. Conversely, the LPI and GYRATE metrics have exhibited an inverse trend. Land cover changes resulted in a 50% and 63% decrease in GYRATE mean, and median values and a 14% and 20% decrease in LPI mean and median values from 2010 to 2035. This denotes that size of patches in the landscape has been decreasing as the number of patches increases.

Disjunct core area density (DCAD) is the only core area metric used in landscape pattern analysis. The mean

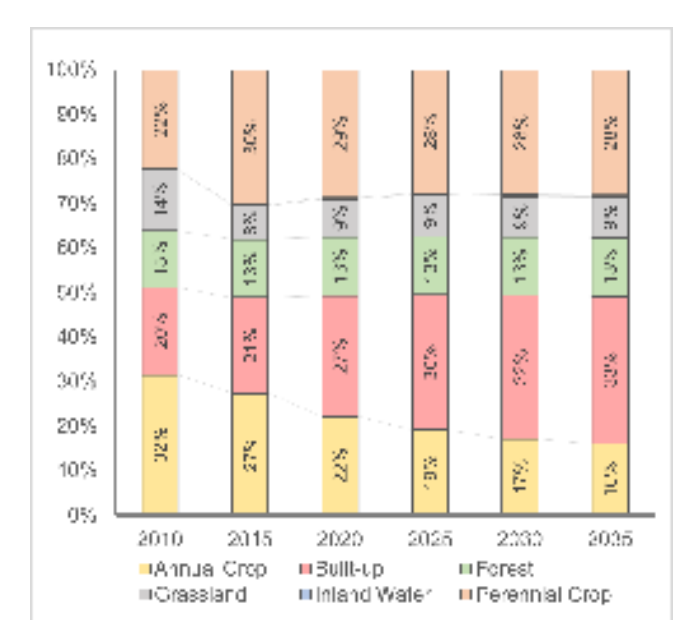


Figure 4. Landscape composition from 2010 to 2035.

DCAD of the catchments in the study area increased by 257%, and its median values increased by 325%. Similarly, the maximum values of the DCAD increased from 254.78 to 764.33. Changes for each period also revealed an increasing trend between 2010–2015, 2015–2020, and 2025–2030. Conversely, decreasing trends trend were observed in the 2020–2025 and 2030–2035 time periods. The trend corroborates the result of

the area-density-edge metrics, which implies a more fragmented landscape.

Contagion-interspersion metrics computed for the study area include the contagion index (CONTAG), aggregation index (AI), landscape division index (DIVISION), and splitting index (SPLIT). The CONTAG metric showed an increase in the mean (*i.e.*, 11% increase) and median (5% increase) values. Likewise, the DIVISION and SPLIT metrics also increased from 2010 to 2035; the means of DIVISION and SPLIT increased by 30% and 38%, respectively, while their medians grew by 32% and 40%. AI did not significantly change throughout all transition periods (*i.e.*, change was less than 1%). Overall, the trends in the metrics indicate that the degree of dispersion and interspersion of patches is increasing.

The value of COHESION from 2010 (99.73) to 2035 (99.42) only changed by less than 1%. Hence it did not significantly change during the period, which means that the connectivity of the patches in the area did not significantly change.

The mean and median values of all the patch diversity metrics increased from 2010 to 2035. Throughout the entire period, the means of PR, PRD, SHDI, and SIDI increased by 32%, 62%, 33%, and 32%, respectively; their median values increased by 33%, 31%, 32%, and 24% respectively. Assessment of changes in each metric

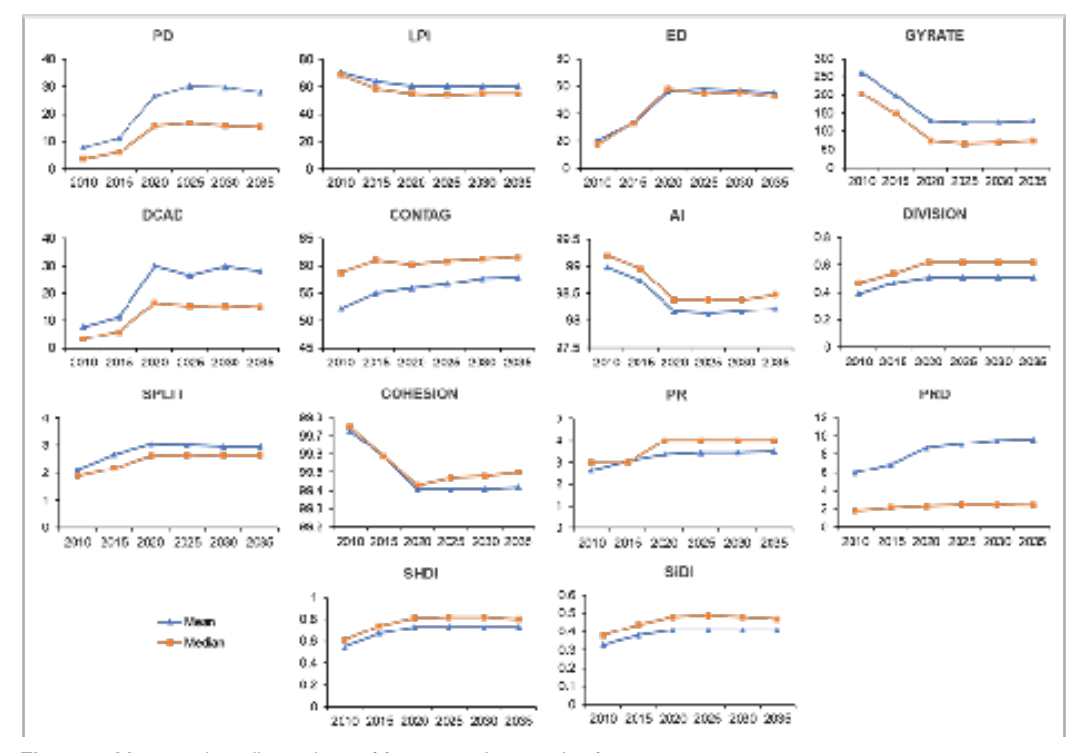


Figure 5. Mean and median values of fragmentation metrics from 2015 to 2035.

for each period also revealed an increasing trend in the mean patch diversity metric values for all transition periods. However, the rates of change in the mean values were decreasing. Similarly, the same trends can be seen for the median values of the metrics, except for the 2025-2030 transition period, where median values of PRD and SIDI each decreased by 1%, and the 2030-2035 transition period, where median values of PRD decreased by 1% and SIDI and SHDI decreased by 3%. Overall, the number of patch types, richness, and evenness increased by 2035.

Interaction of sediment retention and landscape configuration

Multiple linear regression assessed the interaction between the changes in sediment retention and the changes in various landscape pattern metrics. It was also used to measure the degree of influence between the dependent variable (i.e., Δ SRI) and 68 independent variables represented by the landscape level and class level fragmentation metrics (i.e., ΔPD, ΔLPI, ΔED, ΔGYRATE, ΔDCAD, ΔCONTAG, ΔCOHESION, ΔDIVISION, ΔSPLIT, ΔPR, ΔPRD, Δ SHDI, Δ SIDI, Δ AI, etc.). However, the correlation between the independent variables was measured before regression analysis. Correlation analysis of the changes in landscape pattern metrics showed that most were weakly correlated. Overall, only 1% of the correlation coefficients showed a significant correlation (*i.e.*, coefficients greater than 0.8) between metrics. ΔPD and $\Delta DCAD$ were collinear, so ΔPD was not used in the regression. Similarly, the class-level metrics ΔPD_{\perp} AC, $\triangle PD_BU$, $\triangle PD_F$, $\triangle PD_GL$, and $\triangle PD_PC$ were not included in the regression due to their collinearity with ΔDCAD AC, ΔDCAD BU, ΔDCAD F, ΔDCAD GL, and $\Delta DCAD_PC$, respectively. The least correlation was between \triangle PRD and \triangle GYRATE, and \triangle PRD and \triangle SPLIT. The patch diversity metrics were highly correlated, and area-edge metrics were the least correlated.

Multiple regression was used on the variables, and an F-test was conducted on the regression model to assess if the regression coefficients of the independent variables were statistically distinguishable from zero. Since the p-value of the model F-statistic (Prob > F) is equal to 0.0000, the null hypothesis that all coefficients are equal to zero and have a greater than 99.99% confidence that there is a statistically discernible connection between changes in SRI and the changes in various landscape pattern metrics can be rejected. However, the R-square of the model is low, at 0.2054. This implies even though it is statistically significant, the spatial patterns of land cover across the landscape only explain a small percentage of variance in sediment

retention. Hence, landscape composition may play a more considerable impact on the changes in landscape-level ecosystem sediment retention.

Looking at the Beta estimates of the regression line, DIVISION has the highest magnitude of influence per unit change on SRI, followed by AI. However, this may be misleading since the maximum value for both DIVISION, and AI is one. Meaning attaining the highest possible value for DIVISION would increase the SRI value by 0.26, and for AI, it would only increase the SRI value by 0.13. However, the P-value of the said variables indicates low statistical significance at a 95% confidence interval. Statistically significant variables at a minimum of 95% confidence interval are GYRATE, LPI PC, ED AC, ED F, ED GL, and ED PC. Four variables have the highest t-values and the lowest p-values: GYRATE, LPI_PC, ED_AC, and ED_GL. These three variables are statistically significant even at a greater than 99.9% confidence interval.

Computation of the independent variables' variance inflation factor (VIF) revealed that many are collinear, with almost half having VIF >10. The collinear variables were removed to improve the regression model, which resulted in a regression model summarized in Table 6. All the remaining variables have a VIF of five or less, and about 12 variables were statistically significant at a 95% confidence interval (i.e., COHESION, ED_AC, ED_ BU, ED_F, ED_GL, ED_PC, GYRATE, GYRATE_AC, GYRATE_F, GYRATE_PC, LPI_AC, SPLIT). Of these variables, COHESION have the highest regression coefficient, which indicates that for every unit increase, COHESION would result in a 0.07 decrease in SRI. This is followed by SPLIT, which increases SRI by 0.01 for every unit increase. On the other hand, GYRATE_PC has the lowest regression coefficient of 0.00007.

A Moran's I test of spatial autocorrelation was also done by spatially joining the computed datasets of SRI, landscape-level, and class-level fragmentation metrics with their corresponding catchments. The spatial coordinates of each catchment were used to create a neighbors list based on catchments that share at least one boundary using Queen's contiguity criteria (Florax & Rey, 1995). This resulted in 1118 non-zero links between neighbors with a 5.4 average number of links for each catchment; the minimum number of links derived in the neighborhood assessment was two, and the most connected catchment was assessed with 14 links.

A spatial weights matrix was generated for the dataset by assigning weights for each catchment

Table 6. Coefficients, t values, and collinearity of variables in the revised regression model.

M. Zahi.	Standardize	d coefficient		D 111	Collinearity	Collinearity statistics	
Variable -	Value	Std. err.	t	P>Itl	Tolerance	VIF	
ΔDCAD	-0.000668	0.000368	-1.81	0.070	0.205333	4.87	
ΔPRD	0.000896	0.000829	1.08	0.280	0.236922	4.22	
ΔCOHESION	-0.073431	0.030182	-2.43	0.015	0.287689	3.48	
ΔGYRATE_F	0.000275	0.000138	2.00	0.046	0.969213	1.03	
ΔLPI_AC	-0.001917	0.000521	-3.68	0.000	0.513149	1.95	
ΔLPI_BU	-0.000186	0.000632	-0.29	0.769	0.648225	1.54	
ΔSPLIT	-0.014115	0.005653	-2.50	0.013	0.493910	2.02	
ΔED_F	-0.004968	0.001815	-2.74	0.006	0.925325	1.08	
ΔPR	-0.006918	0.008969	-0.77	0.441	0.658827	1.52	
ΔED_AC	0.001561	0.000290	5.38	0.000	0.504455	1.98	
ΔED_PC	-0.000966	0.000230	-4.21	0.000	0.532330	1.88	
ΔGYRATE_GL	0.000018	0.000045	0.41	0.679	0.871652	1.15	
ΔED_GL	0.002617	0.000295	8.87	0.000	0.660283	1.51	
ΔGYRATE	-0.000248	0.000074	-3.38	0.001	0.572332	1.75	
ΔCONTAG	-0.000213	0.000336	-0.63	0.527	0.662981	1.51	
ΔSPLIT_GL	0.000000	0.000000	0.63	0.528	0.988660	1.01	
ΔDCAD_AC	0.000231	0.000744	0.31	0.756	0.541892	1.85	
ΔED_BU	-0.001192	0.000408	-2.92	0.004	0.587441	1.70	
ΔSPLIT_F	0.000000	0.000000	0.20	0.841	0.972300	1.03	
ΔSPLIT_AC	0.000000	0.000000	0.13	0.895	0.993483	1.01	
ΔGYRATE_PC	0.000072	0.000036	1.99	0.047	0.824849	1.21	
ΔGYRATE_AC	0.000106	0.000052	2.04	0.042	0.640094	1.56	
ΔSPLIT_BU	0.000000	0.000000	-0.05	0.959	0.995357	1.00	
ΔDCAD_GL	-0.000231	0.000218	-1.06	0.289	0.779714	1.28	
ΔDCAD_PC	-0.000745	0.000392	-1.90	0.058	0.670509	1.49	
ΔSPLIT_PC	0.000000	0.000000	1.03	0.305	0.998990	1.00	
ΔDCAD_BU	0.000056	0.000587	0.10	0.924	0.813139	1.23	
ΔGYRATE_BU	0.000023	0.000065	0.35	0.727	0.740838	1.35	
_cons	0.007195	0.004264	1.69	0.092	Mean VIF	1.72	

Note: highlighted variables are statistically significant at α =0.05

using the generated neighbors list utilizing a row-standardized scheme. The spatial weights matrix was used in Moran's I test for spatial autocorrelation under randomization, which resulted in a p-value less than 2.2×10^{-16} . This means that the dataset exhibits a statistically discernible level of spatial autocorrelation. The computed Moran's I coefficient was 0.33512, which indicates positive spatial autocorrelation. This is corroborated by the results of Geary's C test for spatial autocorrelation, which showed similar outputs; the p-value was less than 3.452×10^{-6} ; the computed Geary's C statistic was 0.54763.

Similarly, the residuals of the revised regression model were also assessed for spatial autocorrelation using Moran's I test. The results showed statistically significant autocorrelation (p-value = 3.92×10^{-15}) in the residuals of the revised regression model, with Moran's I coefficient equal to 0.31435. A studentized Breusch-Pagan test of the model seems to confirm this, with a p-value of 2.338×10^{-8} and a coefficient of 89.541, which implies heteroskedastic model residuals.

Furthermore, Lagrange Multiplier (LM) diagnostics determined the type of spatial dependence present in the revised regression model. These include the simple LM test for error dependence (LMerr) and the simple LM test for a missing spatially lagged dependent variable (Lmlag). Lmerr and Lmlag showed statistically significant spatial dependence with p-values less

than 6.509 x 10⁻¹³ and 2.7 x 10⁻¹², respectively. Hence, additional LM diagnostics were applied to assess further the type of spatial dependence that would best describe the residuals of the revised regression model. The additional diagnostics tools used were the robust LM test for error dependence in the possible presence of a missing lagged dependent variable (RLMerr), the robust LM test for a missing spatially lagged dependent variable in the possible presence of an error dependent variable (RLMlag); and a portmanteau test (SARMA) which combines both LMerr and RLMlag. RLMerr was the only diagnostic with a statistically significant p-value; thus, the spatial error model was selected as most appropriate for the dataset.

The variables used in the revised regression model were fitted in a spatial error model, and a z-test was conducted to assess if the coefficients of the independent variables were statistically distinguishable from zero. Since the p-value of the model is less than 2.1427×10^{-13} , we can reject the null hypothesis that all coefficients are equal to zero and have a greater than 99.9999% confidence that there is a statistically discernible connection or relationship between changes in SRI and the changes in various landscape pattern metrics.

Furthermore, eight variables (i.e., ED_PC, ED_GL, DCAD_AC, ED_BU, GYRATE_PC, GYRATE_AC, DCAD_GL, and DCAD_PC) were shown to have a statistically significant impact on SRI at a minimum of 95% confidence interval (Table 7). Of these, ED_GL have the highest z-value and the lowest p-value, which indicates statistical significance even at a greater than 99.9999% confidence interval. Looking at the estimated coefficients of the variables, DCAD_AC have the highest magnitude of influence per unit change on SRI a 0.0242 increase in SRI per unit change in DCAD_ AC. This was followed by ED_GL, whose per unit increase also increased SRI by 0.0102. The variables ED_BU, DCAD_GL, and DCAD_PC all have negative coefficients, which indicate a decrease in SRI for every unit increase in the said variables.

Implications and comparison to similar studies

The results of the statistical analysis show that increasing the patch size and ED of built-up areas will result in a decrease in SRI. Conversely, increasing the ED of perennial crops and their average patch size in conjunction with a decreased core area will increase SRI in the landscape. Similarly, decreasing the core area and increasing the ED of grasslands is expected to increase SRI in the study area. Furthermore, increasing the core area of annual crops while increasing its average patch sizes is expected to increase SRI in the landscape. These

metrics imply that to improve sediment retention in the landscape, large and irregular or elongated patches might be a better configuration for perennial crops, irregular or elongated patches for grasslands, while small and compact-shaped patches work best for builtup areas, and large, and compact-shaped patches are optimal for annual crops.

A review article on a meta-analysis of 121 similar studies shows that landscape pattern or landscape complexity has a 29% cumulative mean effect size on water quality-related ecosystem services – an aggregation of nutrient retention, sediment retention, and other related ecosystem services (Duarte *et al.*, 2018). The strongest positive effect was observed for the percentage of noncrop and natural areas, which are composition metrics. For landscape configuration, landscape connectivity positively influenced water quality, while landscape heterogeneity exhibited a significant negative effect. However, this only investigated landscape-level metrics because this had been more prevalent. Hence it is difficult to compare results since class-level metrics were the most influential for the MMFR catchments.

Individual studies on class-level metrics seem to come to different conclusions on landscape configuration and sediment retention. These were also less common; hence a consensus may not have been determined yet. Stepwise regression determined a negative relationship between the aggregation of grasslands and a positive relationship between farmlands' aggregation and ED to sediment retention in the Liaohe River Reserve, China (Xia et al., 2021). Similarly, larger patch sizes, higher aggregation, higher ED, and more compactshaped agricultural areas result in lower sediment yield in the Chenyulan Watershed, Taiwan (Chiang et al., 2019). Both appeared to corroborate this paper's findings. Conversely, in the Blue Nile Basin, the mean patch size and LPI of farmlands and settlements have a negative correlation, while the patch size and LPI of grasslands and the number of farmland patches positively correlated with the decrease in sediment export (Yohannes et al., 2020). Although the patch size and settlement results aligned with the findings in the Blue Nile Basin, its farmland correlations were contrary. Furthermore, grassland results were also similar but were considered statistically insignificant. Only one comparable journal article was performed in the Philippines, a study on sediment yield in the Calumpang Watershed, Batangas (Boongaling et al., 2018). Here, a higher number of patches, a smaller LPI, and less aggregated patches of agriculture were assessed to result in lower sediment yield. For built-up areas, higher aggregation and compact-shaped patches

Table 7. Coefficients, asymptotic standard error, and z-values of variables used in the spatial error model.

Variable	Coefficient	Std. error	z value	Pr >Izl
ΔDCAD	-0.0034483	0.0047016	-0.7334000	0.4632967
ΔPRD	-0.0003846	0.0084534	-0.0455000	0.9637111
ΔCOHESION	-0.1364500	0.1148500	-1.1881000	0.2348087
ΔGYRATE_F	0.0002321	0.0002167	1.0713000	0.2840231
ΔLPI_AC	0.0012178	0.0011926	1.0211000	0.3072279
ΔLPI_BU	0.0016610	0.0014344	1.1580000	0.2468798
ΔSPLIT	-0.0274340	0.0154650	-1.7739000	0.0760822
ΔED_F	-0.0031535	0.0031666	-0.9959000	0.3193079
ΔPR	0.0019165	0.0213510	0.0898000	0.9284780
ΔED_AC	0.0016727	0.0013583	1.2314000	0.2181626
ΔED_PC	0.0024504	0.0010917	2.2446000	0.0247951
ΔGYRATE_GL	-0.0000972	0.0001008	-0.9640000	0.3350305
ΔED_GL	0.0102190	0.0012989	7.8673000	0.0000000
ΔGYRATE_MN	-0.0002334	0.0001868	-1.2494000	0.2115022
ΔCONTAG	0.0000860	0.0008063	0.1066000	0.9150799
ΔSPLIT_GL	0.0000000	0.0000000	-0.2744000	0.7837564
ΔDCAD_AC	0.0242850	0.0089459	2.7146000	0.0066349
ΔED_BU	-0.0038704	0.0012723	-3.0419000	0.0023506
ΔSPLIT_F	0.0000000	0.0000000	0.4304000	0.6668757
ΔSPLIT_AC	0.0000000	0.0000000	0.5406000	0.5887497
ΔGYRATE_PC	0.0002235	0.0000829	2.6974000	0.0069876
ΔGYRATE_AC	0.0002676	0.0001014	2.6392000	0.0083113
ΔSPLIT_BU	0.0000000	0.0000000	0.0755000	0.9398500
ΔDCAD_GL	-0.0064074	0.0018346	-3.4926000	0.0004784
ΔDCAD_PC	-0.0067937	0.0019629	-3.4610000	0.0005381
ΔSPLIT_PC	0.0000000	0.0000000	0.1301000	0.8964925
ΔDCAD_BU	-0.0034762	0.0025619	-1.3569000	0.1748208
ΔGYRATE_BU	0.0001023	0.0001468	0.6972000	0.4856620
(Intercept)	0.0007395	0.0397530	0.0186000	0.9851594

Note: highlighted variables are statistically significant at α =0.05

were deemed to result in lower sediment yield. Their results for built-up areas seem to agree with the results of this paper, but their results for agriculture imply the inverse.

The various methods and metrics used in each study may have influenced the differences in findings. For instance, the initial regression model in this paper had distinct statistically significant variables compared to the final spatial error model, with some even having inverse beta estimates compared to their initial computation. Furthermore, differences in scale may also contribute to the variations. This is because a lot of ecological processes seem to be sensitive to the

scaling of dependent variables, including thematic scale, spatial grain, and spatial extent, among others (Mateo Sánchez *et al.*, 2014; Chambers *et al.*, 2016; Bai *et al.*, 2020; Fu *et al.*, 2021; Li *et al.*, 2022;). Since most other studies were done at a much larger and coarser scale – usually 30 m resolution at a river basin or regional scale compared to 5 m resolution at a catchment scale – this may result in variations in results. Thematic resolution or aggregation of classes also varies in the studies. Hence, this highlights the current limitations of landscape pattern assessment, and this area of research needs further development as new ways of assessing landscape patterns emerge (Gustafson, 2019).

CONCLUSION AND RECOMMENDATIONS

Landscape configuration has been found to have a statistically significant influence on the catchment-level sediment retention of the study area. Although results still need to be verified on the field or by duplicate studies, this holds potential for landscape and watershed management. The spatial error model implies that, to a certain degree, the spatial design and configuration of land use and land cover may also be utilized to improve sediment retention and mitigate soil erosion.

However, even though eight landscape pattern metrics have statistically significant relationships with SRI, the proportion of changes in SRI that can be attributed to the landscape pattern metrics used in the study is less than 5%. It is important to note that landscape composition tends to be the most important indicator of sediment retention for landscape-level interactions. However, at least one study seems to have contradictory results, with landscape configuration being more important. This is a limitation of the study since it looks at the impacts of landscape configuration in isolation of landscape composition. Further investigation should be done by incorporating landscape composition in the statistical analysis to determine its degree of influence on sediment retention vis-à-vis landscape configuration.

Another limitation of the study is that it analyzed a set scale - of 5 m resolution at a catchment scale. A potential area of research missing in this study is the integration of statistical scale screening, selection, or optimization of the landscape pattern metrics. A multiscale analysis optimizes the scale of each variable in the statistical model. This type of multiscale analysis reduces the impact of scale on dependent variables and could potentially improve the comparability of such studies. Lastly, hypothetical land cover pattern generation methods should be explored to assess ecosystem service and landscape pattern relation over a wider range of hypothetical landscape compositions and configurations. Additional studies into this field are warranted, including similar studies on other spatially sensitive ecosystem services. A meaningful understanding of their interaction could be valuable in improving existing measures and developing novel methods and guidelines for soil and water conservation or land use and watershed management planning in the Philippines.

LITERATURE CITED

- Abdolalizadeh, Z., Ebrahimi, A., & Mostafazadeh, R. (2019). Landscape pattern change in Marakan protected area, Iran. *Regional Environmental Change*, 19(6), 1683–1699.
- Adepoju, K., Adelabu, S., & Fashae, O. (2019). Vegetation Response to Recent Trends in Climate and Landuse Dynamics in a Typical Humid and Dry Tropical Region under Global Change. *Advances in Meteorology*, 1–15. https://doi.org/10.1155/2019/4946127>.
- Agudelo, C. A. R., Bustos, S. L. H., & Moreno, C. A. P. (2020). Modeling interactions among multiple ecosystem services. A critical review. Ecological Modelling, 429, 109103. https://doi.org/10.1016/j.ecolmodel.2020.109103.
- Ahmadi M. F., Souri, B., Mohammadzadeh, M., Salmanmahiny, A., & Mirkarimi, S. H. (2018). Evaluation of the relationship between soil erosion and landscape metrics across Gorgan Watershed in northern Iran. *Environmental Monitoring and Assessment*, 190(11), 643.
- Almarines, N. R. (2019). Predicting Spatiotemporal Changes in Land Cover Patterns and Impacts on Sediment Retention of Mt. Makiling Forest Reserve, Philippines [Master's Thesis]. University of the Philippines Los Baños, Philippines.
- Arguelles, E. D. L. R. (2019). New records of corticolous microalgae and cyanobacteria for Philippine algal flora from Mt. Makiling Forest Reserve. *Journal of Microbiology, Biotechnology and Food Sciences*, 9(1), 1–8.
- Auerswald, K., Fiener, P., Martin, W., & Elhaus, D. (2014). Use and misuse of the K factor equation in soil erosion modeling: An alternative equation for determining USLE nomograph soil erodibility values. CATENA, 118, 220–225.
- Benavidez, R., Jackson, B., Maxwell, D., & Norton, K. (2018). A review of the (Revised) Universal Soil Loss Equation ((R)USLE): With a view to increasing its global applicability and improving soil loss estimates. *Hydrology and Earth System Sciences*, 22(11), 6059–6086.
- Boongaling, C. G. K., Faustino-Eslava, D. V., & Lansigan, F. P. (2018). Modeling land use change impacts on hydrology and the use of landscape metrics as tools for watershed management: The case of an ungauged catchment in the Philippines. *Land Use Policy*, 72, 116–128.
- Borselli, L., Cassi, P., & Torri, D. (2008). Prolegomena to sediment and flow connectivity in the landscape: A GIS and field numerical assessment. *CATENA*, 75(3), 268–277.

- Bouguerra, S., Jebari, S., & Tarhouni, J. (2020). Spatiotemporal analysis of landscape patterns and its effect on soil loss in the Rmel River Basin, Tunisia. *Soil and Water Research*, *16*(1), 39–49.
- Castillo, L., Bantayan, N., Canceran, M., Barua, L., Alegre, A., Gonzalvo, K. J., Gestiada, E., Parducho, V., Limpiada, A., & Castillo, M. (2021). Tree composition, diversity, and stand structure of mid-montane forest in Sipit Watershed, Mount Makiling Forest Reserve ASEAN Heritage Park, Philippines. *Philippine Journal of Science*, 150(S1). https://doi.org/10.56899/150.S1.17.
- Chiang, L.-C., Chuang, Y.-T., & Han, C.-C. (2019). Integrating landscape metrics and hydrologic modeling to assess the impact of natural disturbances on ecohydrological processes in the Chenyulan Watershed, Taiwan. *International Journal of Environmental Research and Public Health*, 16(2), 266. https://doi.org/10.3390/ijerph16020266.
- Clanor, M. D. M., Escobar, E. C., Bondad, R. G. M., Duka, M. A., Ventura, J.-R. S., Dorado, A. A., Lu, M. M. D., Sanchez, P., & Mulimbayan, F. (2016). Daily streamflow forecasting of the gauged molawin watershed using model combinations and the ungauged eastern dampalit watershed by spatial proximity regionalization. *Philippine E-Journal for Applied Research and Development*, 6, 19–31.
- Corral-Pazos-de-Provens, E., Rapp-Arrarás, Í., & Domingo-Santos, J. M. (2022). The USLE soil erodibility nomograph revisited. *International Soil and Water Conservation Research*, S2095633922000582. https://doi.org/10.1016/j.iswcr.2022.07.001.
- Craney, T. A., & Surles, J. G. (2002). Model-dependent variance inflation factor cutoff values. *Quality Engineering*, 14(3), 391–403.
- Cushman, S. A., & McGarigal, K. (2019). Metrics and models for quantifying ecological resilience at landscape scales. *Frontiers in Ecology and Evolution*, 7, 440. https://doi.org/10.3389/fevo.2019.00440.
- Dabney, S., Yoder, D., & Vieira, D. (2012). The application of the revised universal soil loss equation, version 2, to evaluate the impacts of alternative climate change scenarios on runoff and sediment yield. *Journal of Soil and Water Conservation*, 67(5), 343–353.
- David, W. P. (1988). Soil and water conservation planning: Policy issues and recommendations. *Journal of Philippine Development*, 15(1), 47–84.
- Desmet, P. J. J., & Govers, G. (1996). A GIS procedure for automatically calculating the USLE LS factor on topographically complex landscape units. *Journal of Soil and Water Conservation*, 51(5), 427.
- Dong, J., Jiang, H., Gu, T., Liu, Y., & Peng, J. (2022). Sustainable landscape pattern: A landscape approach to serving spatial planning. *Landscape Ecology*, *37*(1), 31–42.

- Dormann, C. F. (2007). Effects of incorporating spatial autocorrelation into the analysis of species distribution data. *Global Ecology and Biogeography*, 16(2), 129–138.
- Du, H., Ai, J., Cai, Y., Jiang, H., & Liu, P. (2019). Combined effects of the surface urban heat island with landscape composition and configuration based on remote sensing: A case study of Shanghai, China. *Sustainability*, 11(10), 2890. https://doi.org/10.3390/su11102890.
- Duarte, G. T., Santos, P. M., Cornelissen, T. G., Ribeiro, M. C., & Paglia, A. P. (2018). The effects of landscape patterns on ecosystem services: Metaanalyses of landscape services. *Landscape Ecology*, 33(8), 1247–1257.
- Dubin, R. (2003). Robustness of spatial autocorrelation specifications: Some Monte Carlo evidence. *Journal of Regional Science*, 43(2), 221–248.
- Florax, R. J. G. M., & Rey, S. (1995). The impacts of misspecified spatial interaction in linear regression models. In: Anselin, L., & Florax, R. J. G. M. (eds.), *New Directions in Spatial Econometrics*. pp. 111–135. Springer Berlin Heidelberg. https://doi.org/10.1007/978-3-642-79877-1_5.
- Foster, G., McCool, D., Renard, K., & Moldenhauer, W. (1981). Conversion of the universal soil loss equation to SI metric units. *Journal of Soil and Water Conservation*, 36(6), 355–359.
- Fu, B., Wang, S., Su, C., & Forsius, M. (2013). Linking ecosystem processes and ecosystem services. *Current Opinion in Environmental Sustainability*, 5(1), 4–10.
- Fu, G., Wang, W., Li, J., Xiao, N., & Qi, Y. (2021). Prediction and selection of appropriate landscape metrics and optimal scale ranges based on multiscale interaction analysis. *Land*, 10(11), 1192. https://doi.org/10.3390/land10111192.
- Gao, J., Gong, J., Yang, J., Li, J., & Li, S. (2022). Measuring spatial connectivity between patches of the heat source and sink (SCSS): A new index to quantify the heterogeneity impacts of landscape patterns on land surface temperature. *Landscape and Urban Planning*, 217, 104260. https://doi.org/10.1016/j.landurbplan.2021.104260.
- Gashaw, T., Bantider, A., Zeleke, G., Alamirew, T., Jemberu, W., Worqlul, A. W., Dile, Y. T., Bewket, W., Meshesha, D. T., Adem, A. A., & Addisu, S. (2021). Evaluating InVEST model for estimating soil loss and sediment export in data scarce regions of the Abbay (Upper Blue Nile) Basin: Implications for land managers. *Environmental Challenges*, 5, 100381. https://doi.org/10.1016/j.envc.2021.100381.
- Geary, R. C. (1954). The contiguity ratio and statistical mapping. *The Incorporated Statistician*, *5*(3), 115. https://doi.org/10.2307/2986645.

- Getis, A. (2010). Spatial autocorrelation. *In*: Fischer, M. M., & Getis, A. (eds.), *Handbook of Applied Spatial Analysis*. pp. 255–278. Springer Berlin Heidelberg. https://doi.org/10.1007/978-3-642-03647-7_14.
- Gomes, E., Inácio, M., Bogdzevič, K., Kalinauskas, M., Karnauskaitė, D., & Pereira, P. (2021). Future land-use changes and its impacts on terrestrial ecosystem services: A review. *Science of the Total Environment*, 781, 146716. https://doi.org/10.1016/j.scitotenv.2021.146716.
- Gonzalez, J. C., de Guia, A. P., Dimalibot, J., Pantua, K., Gustilo, W., & Bantayan, N. (2020). Understorey to canopy vertebrate fauna of a lowland evergreen forest in Mt. Makiling Forest Reserve, Philippines. *Biodiversity Data Journal*, 8, e56999. https://doi.org/10.3897/BDJ.8.e56999.
- Gunaratna, N., Liu, Y., & Park, J. (2013). Spatial autocorrelation. *Journal of Recuperado El*, 2, 1–14.
- Gupta, A., Kamble, T., & Machiwal, D. (2017). Comparison of ordinary and Bayesian kriging techniques in depicting rainfall variability in arid and semi-arid regions of north-west India. *Environmental Earth Sciences*, 76(15), 512. https://doi.org/10.1007/s12665-017-6814-3.
- Gustafson, E. J. (2019). How has the state-of-the-art for quantification of landscape pattern advanced in the twenty-first century? *Landscape Ecology*, 34(9), 2065–2072.
- Hamel, P., Chaplin-Kramer, R., Sim, S., & Mueller, C. (2015). A new approach to modeling the sediment retention service (InVEST 3.0): Case study of the Cape Fear catchment, North Carolina, USA. Science of the Total Environment, 524–525, 166–177.
- Hamel, P., Falinski, K., Sharp, R., Auerbach, D. A., Sánchez-Canales, M., & Dennedy-Frank, P. J. (2017). Sediment delivery modeling in practice: Comparing the effects of watershed characteristics and data resolution across hydroclimatic regions. *Science of the Total Environment*, 580, 1381–1388.
- Hasan, S. S., Zhen, L., Miah, Md. G., Ahamed, T., & Samie, A. (2020). Impact of land use change on ecosystem services: A review. Environmental Development, 34, 100527. https://doi.org/10.1016/j.envdev.2020.100527.
- Honkaniemi, J., Rammer, W., & Seidl, R. (2020). Norway spruce at the trailing edge: The effect of landscape configuration and composition on climate resilience. *Landscape Ecology*, 35(3), 591–606.
- Hou, H., & Estoque, R. C. (2020). Detecting cooling effect of landscape from composition and configuration: An urban heat island study on Hangzhou. *Urban Forestry & Urban Greening*, 53, 126719. https://doi.org/10.1016/j.ufug.2020.126719>.

- Javari, M. (2017). Geostatistical modeling to simulate daily rainfall variability in Iran. *Cogent Geoscience*, 3(1), 1416877. https://doi.org/10.1080/23312041.2017.1416877.
- Lee, M.-H., & Lin, H.-H. (2015). Evaluation of annual rainfall erosivity index based on daily, monthly, and annual precipitation data of rainfall station network in Southern Taiwan. *International Journal of Distributed Sensor Networks*, 11(6), 214708. https://doi.org/10.1155/2015/214708>.
- Li, J., Sun, R., Liu, T., Xie, W., & Chen, L. (2021). Prediction models of urban heat island based on landscape patterns and anthropogenic heat dynamics. *Landscape Ecology*, 36(6), 1801–1815.
- Li, J., Xie, B., Gao, C., Zhou, K., Liu, C., Zhao, W., Xiao, J., & Xie, J. (2022a). Impacts of natural and human factors on water-related ecosystem services in the Dongting Lake Basin. *Journal of Cleaner Production*, 370, 133400. https://doi.org/10.1016/j.jclepro.2022.133400.
- Li, J., Zhou, Y., Li, Q., Yi, S., & Peng, L. (2022b). Exploring the effects of land use changes on the landscape pattern and soil erosion of Western Hubei Province from 2000 to 2020. *International Journal of Environmental Research and Public Health*, 19(3), 1571. https://doi.org/10.3390/ijerph19031571.
- Lichstein, J. W., Simons, T. R., Shriner, S. A., & Franzreb, K. E. (2002). Spatial autocorrelation and autoregressive models in Ecology. *Ecological Monographs*, 72(3), 445–463.
- Liu, J., Liu, X., Wang, Y., Li, Y., Jiang, Y., Fu, Y., & Wu, J. (2020). Landscape composition or configuration: Which contributes more to catchment hydrological flows and variations? *Landscape Ecology*, 35(7), 1531–1551.
- Loc, H. H., Irvine, K. N., Suwanarit, A., Vallikul, P., Likitswat, F., Sahavacharin, A., Sovann, C., & Ha, L. (2020). Mainstreaming ecosystem services as public policy in South East Asia, from theory to practice. *In*: Mauerhofer *et al.* (eds.) *Sustainability and Law.* pp. 631–665. Springer Nature Switzerland AG 2020.
- Magcale-Macandog, D. B., Paller, V. G. V., Torreta, N. K., Lambio, I. A. F., Hadsall, A. S., Buot, I., delos Angeles, M. D., Cervancia, C. R., Quiñones, S. G. L., & Laruya, J. M. (2022). Plant diversity of Mount Makiling Forest Reserve: Implications to management and conservation. *In*: Ramamoorthy, S., Buot, I., & Chandrasekaran, R. (eds.), *Plant Genetic Resources, Inventory, Collection and Conservation*. pp. 97–119. Springer Nature Singapore. https://doi.org/10.1007/978-981-16-7699-4_5.
- Martello, F., dos Santos, J. S., Silva-Neto, C. M., Cássia-Silva, C., Siqueira, K. N., Ataíde, M. V. R. de, Ribeiro, M. C., & Collevatti, R. G. (2023). Landscape structure shapes the diversity of plant reproductive traits in agricultural landscapes in the Brazilian

- Cerrado. *Agriculture, Ecosystems & Environment,* 341, 108216. https://doi.org/10.1016/j.agee.2022.108216>.
- McGarigal, K. (2012). Landscape pattern metrics. *In*: El-Shaarawi, A. H., & Piegorsch, W. W. (eds.), *Encyclopedia of Environmetrics* (1st ed.). Wiley. https://doi.org/10.1002/9780470057339.val006.pub2.
- McGarigal, K. (2015). FRAGSTATS: Spatial Pattern Analysis Program for Categorical Maps. University of Massachusetts: Amherst, MA, USA, 182 p.
- Meraj, G., Singh, S. K., Kanga, S., & Islam, Md. N. (2022). Modeling on comparison of ecosystem services concepts, tools, methods and their ecological-economic implications: A review. *Modeling Earth Systems and Environment*, 8(1), 15–34.
- Miles, J. (2014). Tolerance and variance inflation factor. *In*: Balakrishnan, N., Colton, T., Everitt, B., Piegorsch, W., Ruggeri, F., & Teugels, J. L. (eds.), Wiley StatsRef: Statistics Reference Online (1st ed.). Wiley. https://doi.org/10.1002/9781118445112.stat06593.
- Mitchell, M. G. E., Suarez-Castro, A. F., Martinez-Harms, M., Maron, M., McAlpine, C., Gaston, K. J., Johansen, K., & Rhodes, J. R. (2015). Reframing landscape fragmentation's effects on ecosystem services. *Trends in Ecology & Evolution*, 30(4), 190–198. https://doi.org/10.1016/j.tree.2015.01.011.
- Moanga, D. A. (2020). *Modelling Land Use and Land Cover Changes in California's Landscapes*. University of California, Berkeley.
- Nacua, A. E., M. Pacis, H. Y., Manalo, J. R., M. Soriano, C. J., N. Tosoc, N. R., Padirogao, R., E. Clemente, K. J., & Deocaris, C. C. (2018). Short Communication: Macrofungal diversity in Mt. Makiling Forest Reserve, Laguna, Philippines: with floristic update on roadside samples in Makiling Botanic Gardens (MBG). Biodiversitas Journal of Biological Diversity, 19(4), 1579–1585.
- Nedkov, S., Campagne, S., Borisova, B., Krpec, P., Prodanova, H., Kokkoris, I. P., Hristova, D., Le Clec'h, S., Santos-Martin, F., Burkhard, B., Bekri, E. S., Stoycheva, V., Bruzón, A. G., & Dimopoulos, P. (2022). Modeling water regulation ecosystem services: A review in the context of ecosystem accounting. *Ecosystem Services*, 56, 101458. https://doi.org/10.1016/j.ecoser.2022.101458.
- Negese, A. (2021). Impacts of land use and land cover change on soil erosion and hydrological responses in Ethiopia. *Applied and Environmental Soil Science*, 2021, 1–10.
- Oliveira, A. H., da Silva, M. A., Silva, M. L. N., Curi, N., Neto, G. K., & de Freitas, D. A. F. (2013). Development of topographic factor modeling for application in soil erosion models. *In*: Soriano, M. C. H. (ed.), *Soil Processes and Current Trends in Quality Assessment*. *InTech*. https://doi.org/10.5772/54439.

- Paelmo, R. F., Visco, R. G., Landicho, L. D., Cabahug, R. D., Baliton, R. S., Espaldon, M. L. O., & Lasco, R. D. (2015). Analysis of the farmers' knowledge on the ecosystem services of trees in the Molawin-Dampalit Watershed, Makiling Forest Reserve, Philippines. Asia Life Sciences-The Asian International Journal of Life Sciences, 24(1), 169–186.
- Parveen, R., & Kumar, U. (2012). Integrated approach of universal soil loss equation (USLE) and geographical information system (GIS) for soil loss risk assessment in Upper South Koel Basin, Jharkhand. *Journal of Geographic Information System*, 04(06), 588–596.
- Qiu, J., Carpenter, S. R., Booth, E. G., Motew, M., Zipper, S. C., Kucharik, C. J., Loheide II, S. P., & Turner, M. G. (2018). Understanding relationships among ecosystem services across spatial scales and over time. *Environmental Research Letters*, *13*(5), 054020. https://doi.org/10.1088/1748-9326/aabb87.
- Redhead, J. W., Oliver, T. H., Woodcock, B. A., & Pywell, R. F. (2020). The influence of landscape composition and configuration on crop yield resilience. *Journal of Applied Ecology*, 57(11), 2180–2190.
- Remmel, T. K., & Mitchell, S. W. (2021). Landscape pattern analysis. In: Remmel, T. K., & Mitchell, S. W. (eds). *The Routledge Handbook of Landscape Ecology*. pp. 283–311. Tayloar & Francis Group.
- Saidi, N., & Spray, C. (2018). Ecosystem services bundles: Challenges and opportunities for implementation and further research. *Environmental Research Letters*, 13(11), 113001. https://doi.org/10.1088/1748-9326/aae5e.
- Schwab, G. O., Frevert, R. K., Barnes, K. K., & Edminster, T. W. (eds.). (1981). *Soil and Water Conservation Engineering* (3rd ed). Wiley.
- Sharp, R., Chaplin-Kramer, R., Wood, S., Guerry, A., Tallis, H., Ricketts, T., Nelson, E., Ennaanay, D., Wolny, S., Olwero, N., Vigerstol, K., Derric Pennington, Mendoza, G., Aukema, J., Foster, J., Forrest, J., Cameron, D., Arkema, K., Lonsdorf, E., ... Douglass, J. (2018). *InVEST User's Guide*. The Natural Capital Project, Stanford University, University of Minnesota, The Nature Conservancy, and World Wildlife Fund. https://doi.org/10.13140/RG.2.2.32693.78567>.
- Spiegelberg, M., Baltazar, D. E., Sarigumba, M. P. E., Orencio, P. M., Hoshino, S., Hashimoto, S., Taniguchi, M., & Endo, A. (2017). Unfolding livelihood aspects of the Water–Energy–Food Nexus in the Dampalit Watershed, Philippines. *Journal of Hydrology: Regional Studies*, 11, 53–68.
- Srichaichana, J., Trisurat, Y., & Ongsomwang, S. (2019). Land use and land cover scenarios for optimum water yield and sediment retention ecosystem services in Klong U-Tapao Watershed, Songkhla,

- Thailand. Sustainability, 11(10), 2895. https://doi.org/10.3390/su11102895.
- Wischmeier, W. H., Johnson, C. B., & Cross, B. (1971). Soil erodibility nomograph for farmland and construction sites. *Journal of Soil and Water Conservation*, 26, 5189.
- Wischmeier, W. H., & Meyer, L. (1973). Soil erodibility on construction areas. Soil Erosion: causes, mechanisms, prevention and control. *US Highway Research Board Special Report*, 135, 20–29.
- Xia, H., Kong, W., Zhou, G., & Sun, O. J. (2021). Impacts of landscape patterns on water-related ecosystem services under natural restoration in Liaohe River Reserve, China. *Science of the Total Environment*, 792, 148290. https://doi.org/10.1016/j.scitotenv.2021.148290>.
- Yang, R., & Xing, B. (2021). A comparison of the performance of different interpolation methods in replicating rainfall magnitudes under different climatic conditions in Chongqing Province (China). *Atmosphere*, 12(10), 1318. https://doi.org/10.3390/atmos12101318.

- Yohannes, H., Soromessa, T., Argaw, M., & Dewan, A. (2020). Changes in landscape composition and configuration in the Beressa watershed, Blue Nile basin of Ethiopian Highlands: Historical and future exploration. *Heliyon*, *6*(9), e04859. https://doi.org/10.1016/j.heliyon.2020.e04859.
- Zhang, D., Wang, J., Wang, Y., Xu, L., Zheng, L., Zhang, B., Bi, Y., & Yang, H. (2022). Is there a spatial relationship between urban landscape pattern and habitat quality? Implication for landscape planning of the Yellow River Basin. *International Journal of Environmental Research and Public Health*, 19(19), 11974. https://doi.org/10.3390/ijerph191911974.

Annex 1. Equations and descriptions of the landscape pattern metrics used.

Landscape metric	Equation	Description (McGarigal, 2015)
Patch density	$PD = \frac{N}{A}(10,000)(100)$	It is the number of patches of a patch type divided by the total landscape area.
Edge density	$ED = \frac{E}{A}(10,000)$	Is the sum of the lengths (m) of all edge segments divided by the landscape area (m²)
Mean radius of gyration	$GYRATE_MN = \frac{\sum_{p=1}^{N} \frac{\sum_{r=1}^{z} h_{ij}}{z}}{N}$	This is a measure of patch extent; thus, it is affected by both patch size and patch compaction.
Largest patch index	$LPI = \frac{max(a_{ij})}{A}(100)$	A simple measure of dominance, the index quantifies the percent of the total landscape area comprised by the largest patch.
Disjunct core area density	$DCAD = \frac{\sum_{i=1}^{m} \sum_{j=1}^{n} n_{rj}^{c}}{A} (10,000)(100)$	This expresses the number of disjunct core areas on a per unit area basis.
Contagion index	$\textit{CONTAG} = 1 + \frac{\sum_{i=1}^{m} \sum_{k=1}^{n} \left[(P_i) \left(\frac{g_{ik}}{\sum_{k=1}^{m} g_{ik}} \right) \right] \cdot \left[ln(P_i) \left(\frac{g_{ik}}{\sum_{k=1}^{m} g_{ik}} \right) \right]}{2 \ln(m)} \cdot (100)$	It is affected by the dispersion and interspersion of patch types. Hence, if a single class occupies a significant percentage of the landscape, contagion is high.
Aggrega-tion index	$AI = \left[\sum_{i=1}^{m} \left(\frac{g_{ij}}{g_{ij}^{max}}\right) P_i\right] (100)$	It is calculated from an adjacency matrix at the class level which is then aggregated at the landscape level.
Landscape division index	$DIVISION = \left[1 - \sum_{i=1}^{m} \sum_{j=1}^{n} \left(\frac{a_{ij}}{A}\right)^{2}\right]$	It is the cumulative patch area distribution and probability that two random landscape pixels are not in the same patch.
Splitting index	$SPLIT = \left[1 - \sum_{i=1}^{m} \sum_{j=1}^{n} \left(\frac{a_{ij}}{A}\right)^{2}\right]$	Based on the cumulative patch area distribution, it is interpreted as the effective mesh number
Patch cohesion index	$COHES = \left[1 - \frac{\sum_{i=1}^{m} \sum_{k=1}^{n} p_{ij}}{\sum_{i=1}^{m} \sum_{k=1}^{n} p_{ij} \sqrt{a_{ij}}}\right] \left[1 - \frac{1}{\sqrt{A}}\right]^{-1} (100)$	This index at the class level measures the physical connectedness of the corresponding patch type.
Patch richness	PR = m	It is the number of different patch types present within the landscape boundary.
Patch richness density	$PRD = \frac{m}{A}(10,000)(100)$	This standardizes richness to a per area basis that facilitates comparison among landscapes.
Shannon's diversity index	$SHDI = -\sum_{i=1}^{m} (P_i * ln(P_i))$	A measure of diversity applied to landscapes. It is more sensitive to rare patch types than Simpson.
Simpson's diversity index	$SIDI = 1 - \sum_{i=1}^{m} P_i^2$	More intuitive than Shannon, it denotes the probability that 2 pixels would be different patch types.